On the redshift cut-off for flat-spectrum radio sources

Matt J. Jarvis* & Steve Rawlings

Astrophysics, Department of Physics, Keble Road, Oxford, OX1 3RH.

14 May 2007

ABSTRACT

We use data from the Parkes Half-Jansky Flat-Spectrum (PHJFS) sample (Drinkwater et al. 1997) to constrain the cosmic evolution in the co-moving space density ρ of radio sources in the top decade of the flat-spectrum radio luminosity function (RLF). A consistent picture for the high-redshift evolution is achieved using both simple parametric models, which are the first to allow for distributions in both radio luminosity and spectral index, and variants of the $V/V_{\max}$ test, some of which incorporate the effects of radio spectral curvature. For the most luminous flat-spectrum objects, the PHJFS sample is extremely similar to that used by Shaver et al. (1996, 1998) to argue for an abrupt 'redshift cut-off': a decrease by a factor ~ 30 in ρ between a peak redshift $z \sim 2.5$ and $z \sim 5$. Our analysis finds that the observable co-moving volume is too small to make definitive statements about any redshift cut-off for the most luminous flat-spectrum sources, although both constant-ρ (no cut-off) models and models with cut-offs as abrupt as those envisaged by Shaver et al. are outside the 90% confidence region. The inference that the decline in ρ is most likely to be gradual, by a factor ~ 4 between $z \sim 2.5$ and $z \sim 5$, is in accordance with previous work on the RLF by Dunlop & Peacock (1990), but different to the abrupt decline favoured by studies of optically-selected quasars. Dust obscuration provides one explanation for this difference. We show that a significant fraction of the most radio-luminous flat-spectrum objects are Giga-Hertz Peaked Spectrum (GPS) rather than Doppler-Boosted (DB) sources, complicating any interpretation of the redshift cut-off. Studies based on objects extending into the next lower decade of the flat-spectrum RLF are likely to be more fruitful but will require a separation of the GPS and DB populations, careful radio selection and analysis of K-corrections, and larger sky-area redshift surveys than those currently available.

Key words: quasars: general - galaxies:luminosity function, mass function - radio continuum:galaxies

1 INTRODUCTION

A basic question in cosmological research is the redshift, or cosmic epoch, at which the first active galaxies were born. Answering this question is important because active galaxies can have significant impacts on the Universe, for example as a sources of photons for re-ionisation (Haiman & Loeb 1997) and as a source of entropy for the inter-galactic medium (e.g. Valageas & Silk 1999). Distant active galaxies also provide a valuable probe of the formation and early evolution of massive galaxies and their associated dark-matter halos (e.g. Efstathiou & Rees 1988). The differential evo-lution of active galaxies and the global star-formation rate has recently been recognised as a powerful probe of the merger processes which underpin galaxy formation in hierarchical models of structure formation (e.g. Percival & Miller 1999; Cen 2000).

Investigations into the co-moving space density ρ of flat-spectrum radio sources selected at 2.7 GHz (Peacock 1985, hereafter P85; Dunlop & Peacock 1990, hereafter DP90), have found evidence of a large increase in ρ out to redshift $z \sim 2.5$, and seemingly strong evidence for a decline in ρ at higher redshifts. This high-redshift decline, regardless of its magnitude, has come to be known as the 'redshift cut-off', a term which was first introduced by Sandage (1972). Its existence is often used to assert that the $z \sim 2.5$ Universe corresponds to

* Email: mjj@astro.ox.ac.uk

Sample	Area/sr	Sample	$0 < z \leq 1$	$1 < z \leq 2$	$2 < z \leq 3$	$3 < z \leq 4$	$4 < z \leq 5$
PHJFS	3.90	$S_{2.7} > 0.5$ Jy	0	6	10	6	0
SH96[†]	4.0	$S_{2.7} > 0.5$ Jy	0	7	12	6	0
SH96[†]	3.8	$S_{2.7} > 0.25$ Jy	−	−	−	−	0
PSR	0.075	$S_{2.7} > 0.1$ Jy	0	0	0	1	0
P85	0.58	$S_{2.7} > 0.5$ Jy	0	0	3	2	0
PW81	4.05	$S_{2.7} > 1.5$ Jy	0	1	2	0	0
WP85	9.81	$S_{2.7} > 2.0$ Jy	0	6	7	0	0

Table 1: Redshift distributions of the most luminous flat-spectrum sources, as defined in Sec. 2, in various samples selected at 2.7 GHz from the PHJFS, SH96, PSR, P85, PW (Peacock & Wall 1981) and WP85 (Wall & Peacock 1985) samples. The latter three samples were the bright samples used in the DP90 study and the PSR sample combines the Parkes Selected Regions to form the faint sample used by DP90. The † symbol denotes the samples where the spectral index selection criterion of $\alpha_{2.7}^{5.0} \leq 0.4$ was used; the PHJFS and DP90 studies adopted $\alpha_{2.7}^{5.0} \leq 0.5$ as the flat-spectrum criterion. The '−' symbols indicate data yet to be published.

the epoch of maximum quasar activity (e.g. Shaver et al. 1998; hereafter SH98).

Using a 2.7 GHz-selected sample, Shaver et al. (1996; hereafter SH96) suggested a decline in ρ of more than 1 dex between $z \sim 2.5$ and $z \sim 5$ (~ 1.5 dex according to Fig. 1 of SH98), whereas the models of DP90 suggested a much more gradual decline, with behaviour not too far from a roughly constant space density for the most luminous flat-spectrum sources. Understanding this apparent contradiction provided the first motivation for the work described in this paper.

DP90 were the first to suggest that observational data favours a redshift cut-off in the steep- as well as the flat-spectrum population, although their study was subject to a number of uncertainties, most notably a reliance on photometric redshift estimates for a large fraction of their high-redshift sources. Wall & Jackson (1997) and Jackson & Wall (1999) have developed a model which explains the behaviour of both the flat- and steep-spectrum populations using a unification scheme (e.g. Antonucci 1993) in which the flat-spectrum sources are the Doppler-boosted (DB) products of a parent steep-spectrum population in which a redshift cut-off appears as a hard-wired feature. These studies paint a picture of radio source evolution in which a high-redshift redshift cut-off is a natural component (although not an essential component of the Wall & Jackson models; Wall, priv. comm.).

Over the last few years the Oxford group has led programmes aimed at re-investigating this question using redshift surveys of samples selected at low radio frequencies, and hence dominated by the steep-spectrum population (e.g. Rawlings et al. 1998; Willott et al. 1998; Jarvis et al. 1999; Willott et al. 2000; Jarvis et al. 2000). These studies have yet to find any statistical discrimination between models with constant ρ at high-redshift, and those with high-redshift cut-offs. Of course any high-redshift decline in ρ might be quite gradual

or might be a strong function of radio luminosity, so there is not necessarily any fundamental disagreement between this work and claims of redshift cut-offs based on much fainter samples of radio sources (e.g. Dunlop 1998). With these studies in mind, the second motivation of this paper was to determine whether the cosmic evolution of the high-redshift flat-spectrum population provide indirect evidence for a cut-off which, in our opinion, has yet to be established beyond doubt in the parent radio-luminous steep-spectrum population (but see DP90, Dunlop 1998).

As emphasised by P85, DP90, SH96 and others, the crucial advantage of any radio-based work is that with sufficient optical follow-up, it can be made free of optical selection effects, such as increasing dust obscuration at high-redshift. It is chiefly for this reason that the SH96 work is often highlighted as the most convincing evidence to date for the existence of any redshift cut-off for the active galaxy population. Indeed, the similarity of the decline in the ρ of radio sources to those of both optically-selected quasars and to the global star-formation rate has been used (e.g Boyle & Terlevich 1998; Dunlop 1998; SH98; Wall 1998) to suggest a close link between the triggering of starburst and AGN activities, and also to marginalise the effects of dust obscuration on the optically-selected quasar population. However, recent results have cast severe doubts on the veracity of this similarity if there is indeed an abrupt redshift cut-off in the quasar population. The main reason for this is that the most recent versions of the plot of global star-formation rate versus redshift (e.g. Steidel et al. 1999) no longer feature any significant high-redshift decline (c.f. Madau et al. 1996), although gentle declines such as the decline found by DP90 are consistent, within the uncertainties, with a roughly constant rate of star-formation at high-redshift. Recent papers (e.g. Cen 2000) have tended to emphasise and model the difference between the roughly constant star-formation

rate from $z \sim 2$ to $z \sim 4$ and the abrupt redshift cut-off inferred for optically selected quasars. A desire to understand whether this difference is driven by increased dust obscuration at high-redshift provided the third motivation for this paper.

The question of the quasar redshift cut-off is just beginning to be addressed by X-ray surveys, and we can expect rapid advances in this field with the advent of surveys made with Chandra and XMM-Newton. The most recent evaluations of the high-redshift evolution of quasars, based on soft X-ray selected samples (Miyaji, Hasinger & Schmidt 2000), find no firm evidence for an abrupt cut-off. Comparison of the space density at high-redshift from radio and X-ray measurements provided the fourth motivation for this paper.

P85 and SH96 have highlighted the potential problem of spectral curvature and its effect on obtaining reliable $K-$corrections for distant flat-spectrum radio sources: a concave spectral shape means that redshifting produces a systematic increase in the spectral index between two fixed observed frequencies as redshift increases. SH96 used the Gear et al. (1994) study to determine at what redshift z a flat-spectrum source would have an observed spectral index $\alpha_{2.7}^{5.0} > 0.4^{\dagger}$, finding $z \gtrsim 10$. However, Gear et al. observed only DB objects (BL Lacs and OVV quasars), and it was not clear to us that these are necessarily representative of the flat-spectrum population at the highest radio luminosities. Pursuing this worry provided a fifth and final motivation for this paper.

In Sec. 2 we describe the PHJFS sample and how it relates to the studies of P85, DP90 and SH96. In Sec. 3 we highlight the important rôle of the distribution in spectral index to any investigation of the RLF, and of the dangers of using a binned estimation of the RLF. In Sec. 4 we emphasise the importance of spectral curvature. Sec. 5 outlines a simple parametric modelling procedure which incorporates a distribution in spectral index and presents the results of our modelling. In Sec. 6 we use variants of the $V/V_{\max}$ statistic to further investigate the high-redshift space density. In Sec. 7 we attempt to constrain the uncertainties of any high-redshift decline. The implications of our results with particular reference to the five motivations outlined in this Introduction are discussed in Secs. 8 and 9. We review prospects of constraining the space density of flat-spectrum quasars with future redshift surveys in Sec. 10.

We take $H_\circ = 50 \, \mathrm{km \, s^{-1} \, Mpc^{-1}}$ and use two cosmological models: cosmology I is defined by the dimensionless parameters $\Omega_{\mathrm{M}} = 1$ and $\Omega_{\Lambda} = 0$; cosmology

II by $\Omega_{\mathrm{M}} = 0.3$ and $\Omega_{\Lambda} = 0.7$. All radio luminosities quoted are measured in units of $\mathrm{W \, Hz^{-1} \, sr^{-1}}$.

2   THE PARKES HALF-JANSKY FLAT-SPECTRUM SAMPLE

The Parkes Half-Jansky Flat-Spectrum sample (PHJFS) contains 323 sources selected at 2.7 GHz with a flux-density $S_{2.7} > 0.5$ Jy, and a spectral index measured between 2.7 and 5.0 GHz, $\alpha_{2.7}^{5.0} < 0.5$. The survey covers a sky area of 3.90 steradians over all right ascension and declinations $-45° < \delta(1950) < +10°$ excluding galactic latitudes $|b| < 20°$. Most (281) of these sources now have spectroscopic redshifts, a completeness of ≈ 87 percent. We will assume throughout that no significant biases are introduced by this small redshift incompleteness.

We will focus our investigation on the most radio-luminous sources. For cosmology I, we consider the objects with $\log_{10}(L_{2.7}) \geq 27.0$ which isolates approximately the top-decade in luminosity, and is also a very similar criterion to that used by SH96 in their analysis. We also model the RLF in cosmology II with a higher luminosity limit of $\log_{10}(L_{2.7}) \geq 27.3$ which corresponds to the same number of sources present in the analysis for cosmology I, and also corresponds roughly to the top-decade of the RLF. The redshift distributions of the most luminous sources in the PHJFS and of the sample of SH96 are very similar (see Table 1) and a 1-D Kolmogorov-Smirnov test gives a probability of $P_{KS} = 0.99$ suggesting that the redshift distributions are statistically indistinguishable.

It might seem bizarre to concentrate on such a small subset of the total PHJFS sample for our statistical analysis, but the reason for this is that, following SH96, we are seeking *direct* evidence for the decline in the quasar population at high-redshifts. Less radio luminous objects are simply not detectable at high-redshifts in relatively bright samples like the PHJFS. Fig. 1 shows the radio luminosity - redshift ($L_{2.7} - z$) plane for the PHJFS sample including the loci of its $S_{2.7} \geq 0.5 \, \mathrm{Jy}$ flux-density limit at three different values of α. For an $\alpha \sim 0$ source the maximum observable redshift of a source at the PHJFS flux-density limit and our adopted luminosity limit is four, and this redshift limit drops precipitously as the critical luminosity is lowered.

Obviously many of the PHJFS sources will also be present in the SH96 sample, due to the overlap in sky area and the similar flux-density limit. Indeed $\approx 65\%$ of the sky-area covered by the PHJFS is also covered by the $S_{2.7} > 0.5$ Jy sample of SH96. Therefore one would expect at least ≈ 14 of the most luminous sources in the PHJFS to be included in the SH96 sample. Although one might expect to find a few more sources in total in the SH96 sample due to the incompleteness of the PHJFS. The overlap with the samples used by DP90

† We use the spectral index convention $S_\nu \propto \nu^{-\alpha}$, where S_ν is the flux-density at the observing frequency ν.
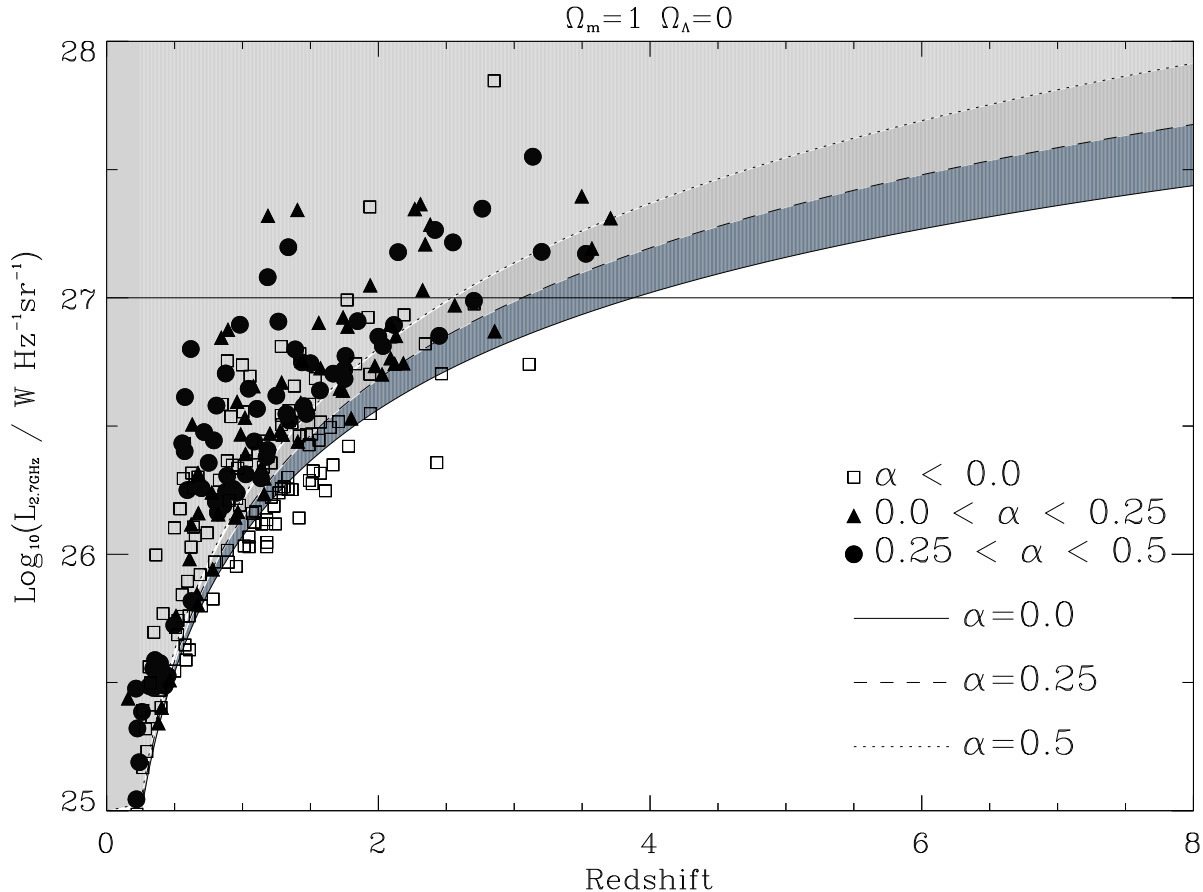
Figure 1: The rest-frame 2.7 GHz radio luminosity $L_{2.7}$ versus redshift z plane for the PHJFS sample for cosmology I. The horizontal solid line shows the lower luminosity limit in cosmology I. The solid curve corresponds to the lower limit in luminosity for sources with $\alpha = 0.0$, the dotted line for sources with $\alpha = 0.25$ and the dashed line for sources with $\alpha = 0.5$. The shaded regions show where sources at the flux-density limit ($S_{2.7} \geq 0.5$ Jy) are permitted to lie. The filled circles represent sources from the PHJFS with radio spectral indices in the range $0.25 < \alpha < 0.5$; filled triangles, $0.0 < \alpha < 0.25$; and open squares, $\alpha < 0.0$, i.e. the inverted-spectrum sources.

will be less (~ 50 %) due to their use of the comparatively deep $S_{2.7} > 0.1$ Jy Parkes selected region (1 source in common), and poor sky overlap with some of the brighter samples. Of the 22 PHJFS objects considered here, 7 sources are in common with the sample of WP85, 3 sources with P85, and the $S_{2.7} > 1.5$ Jy sample has no overlap with the PHFJS as it only covers declinations $\delta > 10°$.

3   THE IMPORTANCE OF MODELLING THE SPECTRAL INDEX DISTRIBUTION AND THE RLF

The name 'flat-spectrum quasar' unfortunately carries with it the implication that $\alpha \sim 0$ so that the flux-density, and hence the luminosity, is more-or-less independent of frequency. One might naively expect that $K-$corrections are therefore unnecessary, or of marginal significance. As quantified by P85, even with the smooth and fairly flat spectra of interest, this is not the case.

There are a finite number of radio-luminous flat-spectrum sources observable on our light cone. The flux-density limit of a survey means that only a fraction of these objects will make it into the survey once the redshift exceeds a critical value given by the intersection of the horizontal line in Fig. 1 and the relevant flux-density limit. Fig. 3 illustrates this fraction as a function of redshift assuming a power-law RLF of steepness β (see eqn. 2) and a mean radio spectral index α. For a given β at any given redshift above $z \sim 2.5$, the observable fraction of the most luminous sources is a strong function of spectral index because of the larger cosmological volume available to the flatter-spectrum sources on our light cone (see Fig. 1). A second more subtle effect concerns β: at fixed α and z, again assumed to be above $z \sim 2.5$, the fraction of sources in the survey drops dramatically with β because more luminous sources can be seen over larger cosmological volumes, and β determines the relative numbers of sources as a function of luminosity. In the extreme case of a very
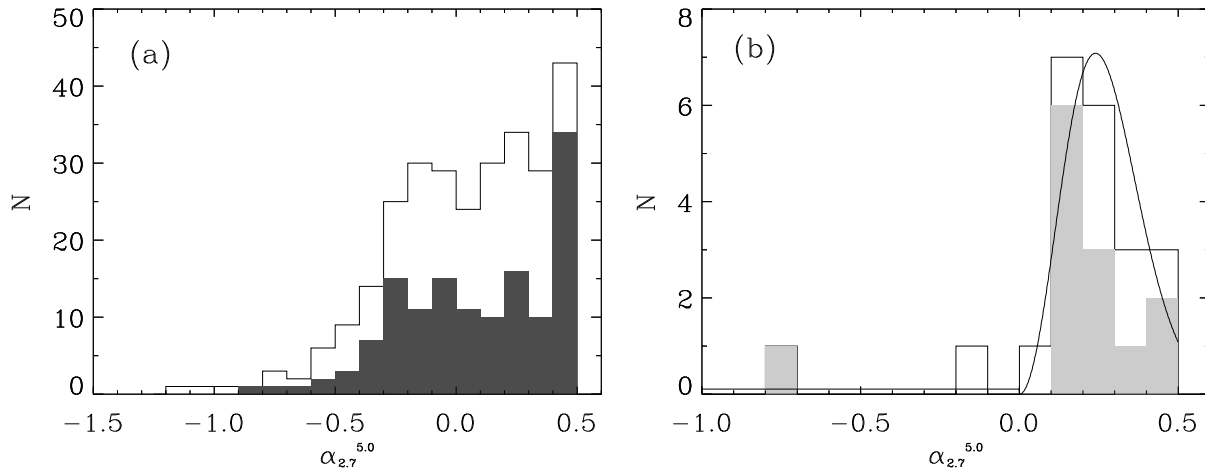
Figure 2: (a) Distribution in observed spectral index between 2.7 and 5 GHz ($\alpha_{2.7}^{5}$) for the whole of the PHJFS sample with spectroscopic redshifts. The dark-shaded region shows the distribution for sources with $z < 1$. (b) Distribution in α for sources from the PHJFS with $\log_{10}(L_{2.7}) \geq 27.0$ for cosmology I. The curve shows the functional form used to parameterise the distribution in α with the fitted values from model A (Sec. 5) with the light-shaded region shows the sources with $z < 2.5$.
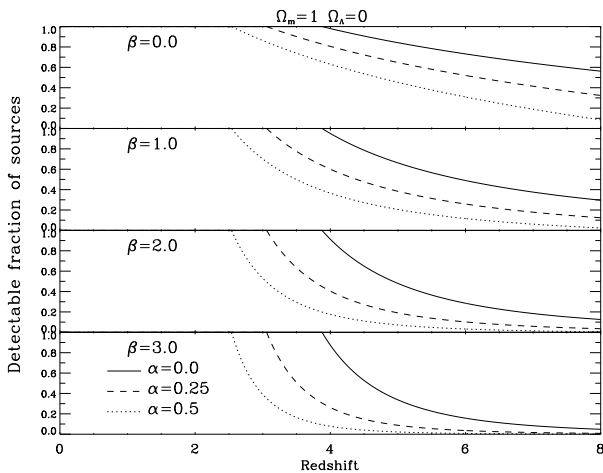

Figure 3: The fraction of luminous ($\log_{10}(L_{2.7}) > 27$) sources on our light cone with $S_{2.7} = 0.5$ Jy and spectral index α detectable in a flux-density limited sample of $S_{2.7} \geq 0.5$ Jy, weighted according to various power-law RLFs (each with index β, see eqn. 2) for cosmology I.

steep RLF ($\beta \sim 3$), and $\alpha \sim 0.5$, for example, there is effectively zero available volume on our light cone in which to detect the most radio luminous flat-spectrum sources beyond $z \sim 4$. The lack of very high-redshift quasars in a sample might be telling us more about the lack of observable volume than about an intrinsic lack of objects.

The analysis of the most radio luminous population by SH96 and SH98 adopted the median spectral index of their large sample, namely $\alpha = 0$ (Shaver, priv. comm.). However, focusing on the most-luminous sources in the PHJFS we see from Fig. 1, and clearer still in the histograms plotted in Fig. 2, that their spectral index dis-

tribution (Fig. 2b) is dissimilar to the distribution for the whole sample (Fig. 2a): Fig. 2a is a broad distribution with a mean spectral index of $0.04(\pm 3\%)$ whereas Fig. 2b has a sharp peak with a significantly steeper mean spectral index of $0.19(\pm 5\%)$; there is still a tail of sources with inverted spectra in Fig. 2b but it includes only 9 per cent of the population whereas, in Fig. 2a, 43 per cent are inverted. A 1-D Kolmogorov-Smirnov test gives a probability $P_{KS} \sim 10^{-3}$ that the two α distributions shown in Figs. 2a and 2b are different. Fig. 2a, shows the distribution in spectral index for sources with $z < 1$ (roughly half the sources) which, being similar to the distribution as a whole ($P_{KS} = 0.41$), suggests no gross dependence of the spectral index distribution on redshift. Similarly Fig. 2b shows the distribution of the most luminous sources with $z < 2.5$ (again roughly half the sources) and once more the distribution is consistent with the most luminous sources as a whole ($P_{KS} = 0.99$), and no gross redshift-dependent effect is apparent. Although redshift effects may play an important rôle in determining the spectral index distribution of the sample, and the analysis presented here falls far short of a thorough investigation of the various inter-correlations, it is hard to escape the conclusion that the correlation between luminosity and spectral index is the dominant factor in skewing the distribution in α for the most radio luminous sources. We will suggest a probable cause for this effect in Sec. 8.2. Because the mean of the distribution in Fig. 2b, i.e. $\alpha = 0.19(\pm 5\%)$, is significantly different to the $\alpha = 0$ adopted by SH96, there will be a significant reduction in the observable co-moving volume of the most radio luminous flat-spectrum sources at high-redshift (c.f. Fig. 3).

The analyses of SH96 and SH98 employed a bin-

ning method for their study of the most luminous flat-spectrum radio sources. The finite size of the bins in radio luminosity can also lead to systematic effects. Consider the extreme example of analysing the $27.0 \leq \log_{10}(L_{2.7}) \leq 28.0$ region of the PHJFS sample as a single luminosity bin. Assigning $\log_{10}(L_{2.7}) = 27.5$ as the characteristic luminosity of this bin would mean that the observable volume would tend to be greatly over-estimated: the steepness of the RLF means that most of the sources in the relevant luminosity bin could only be observed over a much lower cosmological volume. This would lead to an estimate of space density that was systematically biased to low values. The influence of β on the fraction of luminous objects observable has already been shown in Fig. 3.

To summarise, we have identified in this section two possible systematic effects in the SH96 and SH98 analyses which would tend to bias their derived high-redshift space densities to low values. To quantify these effects we use parametric models for the RLF (Sec. 5) which include a distribution in α, and which take account of the steepness of the RLF.

4   THE EFFECTS OF SPECTRAL CURVATURE

The radio spectra of the most luminous PHJFS sources (Fig. 4) show that, as suggested by Savage & Peterson (1983), P85 and SH96, spectral curvature needs to be considered. In this short section we quantify how this might influence searches for very high-redshift quasars at high (2.7 GHz) radio frequencies.

By fitting the spectra in Fig. 4 with a polynomial of the form $y = \log_{10} S_\nu = \sum_{i=0}^{2} a_i x^i$, where $x = \log_{10}(\nu/\text{GHz})$, we find that $\approx 70\%$ of the spectra become steeper with increasing frequency with mean values of $a_1 = 0.07 \pm 0.08$ and $a_2 = -0.29 \pm 0.06$. If we now use these mean values as representative of a source at $z \simeq 2.5$ then we find that it would have an observed spectral index between 2.7 and 5.0 GHz $\alpha_{2.7}^{5.0} \simeq 0.26$ which is similar to the mean of our sample just as one would expect. If we now shift this source out to $z = 5$ then it would have steepened to $\alpha_{2.7}^{5.0} \simeq 0.4$. The mean spectral index will therefore increase systematically with redshift when the effects of spectral curvature are considered and, as we will show in Sec. 10, even small systematic shifts can produce significant effects. Sources at $z \geq 5$ in a flux-density limited sample are likely to have significantly reduced observable volumes (see Fig. 3) as a result of spectral curvature, and also in some cases to become so steep that they fail the filtering criteria of the survey: current searches for high-redshift flat-spectrum quasars (e.g. SH96) do not include sources whose observed spectra are steeper than a critical value around 0.4.

5   PARAMETRIC RLF MODELLING

5.1   Method

Parametric models provide an effective method of extracting as much information as possible from a small dataset, and according to Occam's razor we need to favour the simplest model consistent with the data; in practice, this requires us to restrict the models to as few free parameters as possible. An alternative approach is to use a 'free-form' fit (Peacock & Gull 1981; P85; DP90) which has the advantage of making more general assumptions about the functional forms of the model RLFs, but which with the small dataset of interest here would require the use of such low-order 'free-form' polynomial expansions that it would end up using functional forms which are very similar to those we explicitly consider.

To investigate the RLF of the most-luminous flat-spectrum quasars we considered six models with common parameterisations for the radio luminosity dependence and spectral index distribution, but differing parameterisations for the redshift evolution. That is we look for a separable distribution function of the form

$$\rho(L_{2.7}, z, \alpha) = \rho_\circ \times \rho_L(L_{2.7}) \times \rho_X(z_N) \times \rho_\alpha(\alpha), \qquad (1)$$

where the normalising factor $\rho_\circ$ is a free parameter measured in units of Mpc^{-3} and $\rho_L(L_{2.7})$, $\rho_X(z)$ and $\rho_\alpha(\alpha)$ are dimensionless distribution functions per $(\Delta \log_{10} L_{2.7})$, per (Δz), and per $(\Delta \alpha)$ respectively. Our treatment of a distribution in α means that our definition of ρ differs from that employed by, for example, DP90.

It is highly improbable that the true distribution function is separable since there are likely to be cross-correlations between $L_{2.7}$, z and α from both physical and K-correction effects. However, by confining our attention to a narrow range in $L_{2.7}$, the influence of such cross-correlations are minimised, and our assumed separable form is likely to be an adequate approximation. The alternative of encoding correlations into the functional form would introduce too many additional free parameters for the small dataset under study. We return to the possible influence of z–α correlations in Sec. 10 when we consider searches for flat-spectrum quasars at $z > 5$.

We use a single power-law to parameterise $\rho(L_{2.7})$, i.e.

$$\rho_L(L_{2.7}) = \left(\frac{L_{2.7}}{L_\circ}\right)^{-\beta}, \qquad (2)$$

where β is a dimensionless free parameter, $L_{2.7}$ is the rest-frame 2.7 GHz luminosity and $L_\circ$ is a normalising luminosity fixed at the lower luminosity limit of the sample of the most luminous sources (different for each cosmology). We parameterise the distribution of spectral indices with
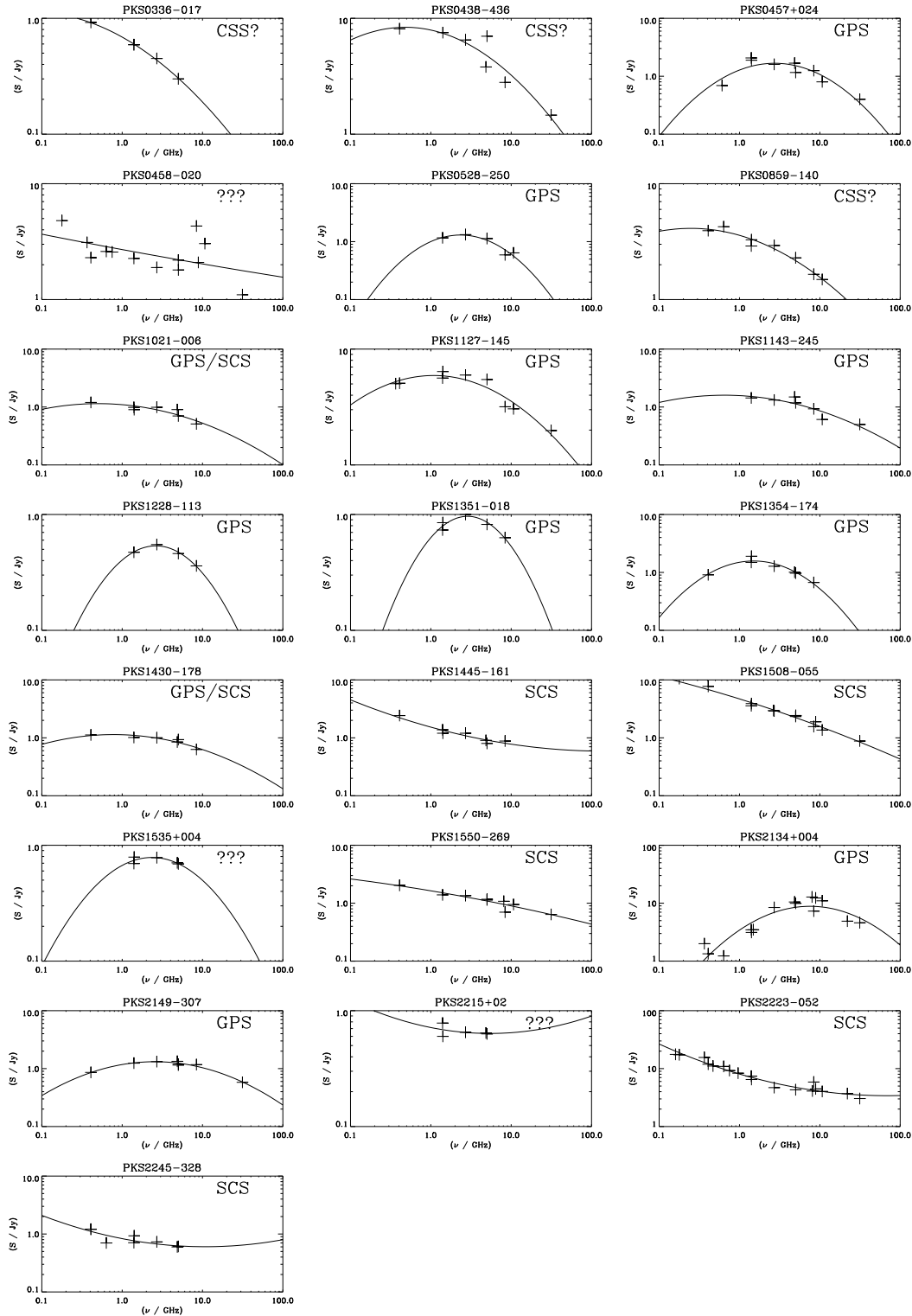
Figure 4: Radio spectra of the most luminous sources from the PHJFS. We have roughly classified each spectrum according to the following scheme: GPS = Giga-Hertz Peaked Spectrum; CSS? = possible Compact Steep Spectrum, spectrum peaking below 0.5 GHz; SCS = Straight or Concave Spectrum; GPS/SCS = GPS or SCS (more observations needed to clarify); and ??? = not classified due to insufficient data. The curves show the fits described in Sec. 4.

$$\rho_\alpha(\alpha) = \begin{cases} \alpha^2 \exp(-\gamma\alpha^2) & : \quad \alpha > 0.0 \\ \epsilon & : \quad \alpha \leq 0.0, \end{cases} \quad (3)$$

where γ and ϵ are free parameters in the model fitting. We now describe the redshift distributions for the six models. Model A is parameterised by a single Gaussian distribution in redshift which (at least in cosmology I) is consistent with the shape of the evolution in co-moving space density of the most luminous flat-spectrum sources suggested by SH96, and also with some derivations of the evolution of optically-selected quasars (see Fig. 3 of SH96). The form used forces a decline at high redshifts, i.e.

$$\rho_A(z) = \exp\left\{ -\frac{1}{2}\left(\frac{z - z_\circ}{z_1}\right)^2 \right\}, \quad (4)$$

where $z_\circ$ is the redshift of the Gaussian peak and z_1 is the characteristic width of the Gaussian. Note that an undesirable feature of this functional form is that it enforces a symmetry about z_0 which couples the decay rates at low- and high-redshift for which there is no physical justification.

Model B is parameterised by a Gaussian which becomes constant beyond its peak, i.e.

$$\rho_B(z) = \begin{cases} \exp\left\{ -\frac{1}{2}\left(\frac{z - z_\circ}{z_1}\right)^2 \right\} & : \quad z \leq z_\circ \\ 1.0 & : \quad z > z_\circ, \end{cases} \quad (5)$$

where $z_\circ$ and z_1 are as previously defined. These two forms have also been used by Willott et al. (1998) in their study of the RLF of steep-spectrum radio quasars.

Models C-E use cut-offs at high- and low-redshift set to be equal to relevant dynamical time-scales. At low-redshifts we use $t_{clus} = 4 \times 10^9$ yr, the dynamical time-scale for a massive ($\sim 10^{15}\,M_\odot$) cluster, as the width of a Gaussian in redshift space where the activity has fallen by a factor of ~ 100 from the fitted peak. The rationale for this is that the cause of the low-redshift decline in ρ seems to be linked to the virialization of rich clusters (e.g. Ellingson, Green & Yee 1991, Rees 1995) since galaxy mergers, the probable trigger mechanism for powerful radio activity, are suppressed in such environments. This assumption is somewhat arbitrary, but serves to eliminate fitting problems with setting the model ρ precisely to zero at some redshift, and also clearly decouples the low-redshift evolution from the high-redshift evolution.

Model C parameterises the low-redshift cut-off as just described, and fits the high-redshift evolution with a half Gaussian above a fitted peak, i.e.

$$\rho_C(z) = \begin{cases} \exp\left\{ -\frac{1}{2}\left(\frac{z - z_\circ}{z_{clus}/2.58}\right)^2 \right\} & : \quad z \leq z_\circ \\ \exp\left\{ -\frac{1}{2}\left(\frac{z - z_\circ}{z_1}\right)^2 \right\} & : \quad z > z_\circ, \end{cases} \quad (6)$$

where $z_\circ$ and z_1 are again the peak and width of the Gaussian; z_{clus} corresponds to a time t_{clus} after the

peak where the activity has decreased by $\approx 99\%$. The factor of 2.58 reduces the width of the Gaussian to a value which corresponds to the inclusion of 99 per cent of the area of the full Gaussian for the given time-scale in redshift space.

Model D again uses t_{clus} to set the rate of the low-redshift decline but forces the distribution to a constant above a fitted $z_\circ$, i.e.

$$\rho_D(z) = \begin{cases} \exp\left\{ -\frac{1}{2}\left(\frac{z - z_\circ}{z_{clus}/2.58}\right)^2 \right\} & : \quad z \leq z_\circ \\ 1.0 & : \quad z > z_\circ, \end{cases} \quad (7)$$

where the symbols are consistent with those used in Model C. Note that this model uses only five free parameters.

For model E we use $t_{gal} = 3 \times 10^8$ yr, the dynamical time-scale of a massive ($\sim 10^{12}\,M_\odot$) galaxy, to set the decay rate of the high-redshift cut-off. Again this choice is somewhat arbitrary, but the rationale is that the cut-off at high-redshift is probably linked to the formation of the first massive galaxies (e.g. Rees 1995), and their dynamical time-scale sets the fastest rate at which the cut-off can decline. Below the fitted peak $z_\circ$ this model is again constrained by t_{clus} and above $z_\circ$ this model becomes constant until it reaches z_1 where it declines as a Gaussian, i.e.

$$\rho_E(z) = \begin{cases} \exp\left\{ -\frac{1}{2}\left(\frac{z - z_\circ}{z_{clus}/2.58}\right)^2 \right\} & : \quad z \leq z_\circ \\ 1.0 & : \quad z_\circ < z < z_1 \\ \exp\left\{ -\frac{1}{2}\left(\frac{z - z_\circ}{z_{gal}/2.58}\right)^2 \right\} & : \quad z \geq z_1, \end{cases} \quad (8)$$

where z_{gal} is the width in redshift space which corresponds to t_{gal} beyond the peak where the activity has decreased by a factor of ≈ 99.

Finally model F fixes the space density to be constant with redshift over all redshifts, i.e.

$$\rho_F(z) = 1.0. \quad (9)$$

This model will be used to illustrate the problem of dealing with small number statistics at low- and high-redshift where the observable co-moving volume is low. Note that this model has only four free parameters.

We used the maximum likelihood method of Marshall et al. (1983) to find best-fit parameters for all six models. If we define S as $-2\ln\mathcal{L}$, where $\mathcal{L}$ is the likelihood function, then by minimising S we find the best-fit values for the free parameters. S is given by,

$$S = -2\sum_{i=1}^{N} \ln[\rho(L_{2.7_i}, z_i, \alpha_i]$$

$$+2\iiint \rho(L_{2.7}, z, \alpha)\Omega(L_{2.7}, z, \alpha)$$

$$\times \frac{dV}{dz}dz\,d(\log_{10} L_{2.7})\,d\alpha, \quad (10)$$

where $\rho(L_{2.7}, z, \alpha)$ is the model distribution,

$\Omega(L_{2.7}, z, \alpha)$ is the sky area available (in sr) for samples of a given flux-density and spectral index cut-off, and $(\mathrm{d}V/\mathrm{d}z)$ is the differential co-moving volume element per steradian. The first term is simply the sum over the N sources in the defined sample. The second term is the integrand of the model distribution and should yield $\approx 2N$ for good fits. A downhill simplex routine was used to minimise eqn. 10 to find the best-fit parameters. The errors associated with these parameters were found by numerically calculating the components of the *Hessian* matrix ($\nabla\nabla S$) at the location of the minimum, inverting this matrix to obtain the covariance matrix ($[\sigma^2]_{ij} = 2[(\nabla\nabla S)^{-1}]_{ij}$) and taking the 1σ errors as given by the square root of the diagonal elements of this matrix (e.g. Sivia 1996).

To determine whether the best-fit models are reasonable fits to the data we used 1- and 2-D Kolmogorov-Smirnov (KS) tests (Peacock 1983) on projections of the data. From these we determined the probability P_{KS} that the model distribution is a fair representation of the data; note that in cases where the probability $P_{KS} > 0.2$, the model and data are statistically indistinguishable, and that higher values of P_{KS} are not necessarily suggestive of better fits (see Press et al. 1992).

To obtain relative probabilities for each model we used the procedure set out in Sivia (1996). Briefly, for the models under consideration the ratio of posterior probabilities of model X relative to model C is given approximately by

$$P_{\mathrm{R}} = \frac{P(\mathrm{X}\,|\,\mathrm{data})}{P(\mathrm{C}\,|\,\mathrm{data})} = \frac{e^{\frac{-S_{X|\mathrm{min}}}{2}}\sqrt{\mathrm{Det}(\nabla\nabla S_C|_{S_{\mathrm{min}}})}}{e^{\frac{-S_{C|\mathrm{min}}}{2}}\sqrt{\mathrm{Det}(\nabla\nabla S_X|_{S_{\mathrm{min}}})}} \times \mathcal{F}, \quad (11)$$

where $\mathrm{Det}(\nabla\nabla S_X|_{S_{\mathrm{min}}})$ is the determinant of the Hessian matrix for model X, evaluated at $S = S_{\mathrm{min}}$ and prior ranges for free parameters common to all models (e.g. those of $\log_{10}\rho_\circ$, β, γ and ϵ) have been cancelled. $\mathcal{F}$ is a factor which compensates for the varying number of parameters between models, and for model F, for example is

$$\mathcal{F} = (4\pi)^{\frac{N-6}{2}}\Delta z_\circ \Delta z_1,$$

where N is the number of free parameters (i.e. 4 for model F) and $\Delta z_\circ \Delta z_1$ is the multiple of the prior ranges for any additional parameters in model C (with respect to model F [‡]). In all cases considered here, this additional factor $\mathcal{F}$ is of order unity and may be ignored.

5.2 Results

Table 2 shows the relative probabilities P_{R} of models A–F normalised to model C. These results demonstrate

---

[‡] Note that in a comparison of model D with model C this multiple of the prior ranges would become just Δz_1.

that none of the best-fit parameterisations illustrated in Fig. 7 are unequivocally ruled out. Moreover, for all of our models the 2D KS-test produces $P_{KS} > 0.2$ for the $L_{2.7} - z$ plane signifying that all our models are reasonable approximations to the data, and the 1D KS-test produces in all cases $P_{KS} \approx 0.48$ for the α distribution again suggesting a good working model (see Fig. 2b). All these statements are true in both cosmology I and cosmology II. We see that the normalisation ρ_0 and slope of the RLF β are consistent between the models as expected if all the fits are reasonable. These values are also in good quantitative agreement with those determined by DP90: their Fig. 11 suggests $\beta \approx 1.3$, and integrating eqn. 3 over α produces values of ρ at a given z within a factor of two of those derived by DP90.

Considering models A and B, we see that any marginal preference for A largely disappears on changing from cosmology I to cosmology II. Model A, which has a Gaussian distribution for its redshift evolution, probably gives a false indication of the steepness of any decline in ρ at high-redshift. This is due to the coupling of the low- and high-redshift declines introduced by the assumed Gaussian distribution: the lack of sources below $z \leq 1$, and the flat behaviour over $1 \leq z \leq 4$ forces the Gaussian to have a very narrow width which is then imposed at the high-redshift end of the function. This effect is highlighted in model B where the high-redshift evolution is characterised by a constant co-moving space density and is not dependent on the width of the fitted Gaussian at low-redshift. The fitted width of this Gaussian is extremely narrow due to the dramatic decline at low-redshift.

Model C removes the coupling of the low- and high-redshift behaviour present in model A but still fits a variable form at high-redshift. Fig. 7 shows the shallowness of the decline in this model. Comparing model C with model D, its no cut-off counterpart, we find no evidence to suggest that the cut-off model is a significantly better representation of the data. The relative probabilities are 0.5 and 0.65 in favour of the Gaussian decline in cosmology I and II respectively.

Consideration of model E in which rapid (but different) declines are enforced at low- and high-redshift, shows a steep increase in co-moving space density from $z = 0$ to $z \approx 1.4$, followed by a constant co-moving space density up to $z \approx 3.5$. Beyond $z \approx 3.5$, i.e. the highest redshift object in the sample, the data are well fitted by a very abrupt cut-off. Indeed, this has the highest probability of all the models considered. This is suggestive of a decline in the co-moving space density at $z \gtrsim 3.5$ and provides the only evidence from our simple parametric models for a redshift cut-off, with the ratio of the probabilities between the worst-fit (model B) and the best-fit (model E) models for cosmology I of ~ 10. There is, however, a way in which the statistical likelihood of cut-off models might have been systematically over-estimated, namely the effects of curvature in the

Model	Cos	N	$\log_{10}\rho_\circ$	β	$z_\circ$	z_1	γ	$\log_{10}\epsilon$	$S_{\min}$	$\ln\mathrm{Det}(\nabla\nabla S)$	P_{R}
A	I	6	-7.29 ± 0.18	1.30 ± 0.39	2.58 ± 0.22	0.87 ± 0.18	17.5 ± 3.7	-3.26 ± 0.35	1037.67	29.38	0.85
B	I	6	-7.42 ± 0.17	1.75 ± 0.34	1.19 ± 0.10	0.05 ± 0.14	16.4 ± 3.6	-3.47 ± 0.35	1043.95	25.40	0.27
C	I	6	-7.33 ± 0.18	1.33 ± 0.41	1.49 ± 0.18	1.74 ± 0.50	17.6 ± 3.67	-3.28 ± 0.35	1038.68	28.05	1.0
D	I	5	-7.43 ± 0.17	1.74 ± 0.39	1.40 ± 0.18	—	16.4 ± 3.6	-3.46 ± 0.35	1045.34	22.77	0.5
E	I	6	-7.50 ± 0.19	1.19 ± 0.40	1.43 ± 0.18	3.38 ± 0.15	16.1 ± 3.7	-2.99 ± 0.29	1032.22	31.68	4.1
F	I	4	-7.52 ± 0.17	1.66 ± 0.39	—	—	16.7 ± 3.6	-3.44 ± 0.35	1051.74	16.37	0.5
A	II	6	-7.88 ± 0.18	1.30 ± 0.38	2.53 ± 0.24	0.92 ± 0.21	17.4 ± 3.7	-3.27 ± 0.35	1095.63	28.94	0.92
B	II	6	-7.97 ± 0.18	1.75 ± 0.34	1.18 ± 0.16	0.05 ± 0.28	16.3 ± 3.8	-3.51 ± 0.35	1101.29	23.69	0.75
C	II	6	-7.89 ± 0.18	1.33 ± 0.40	1.37 ± 0.14	1.80 ± 0.50	17.4 ± 3.7	-3.29 ± 0.35	1095.97	28.44	1.0
D	II	5	-7.97 ± 0.17	1.74 ± 0.38	1.32 ± 0.16	—	16.3 ± 3.5	-3.51 ± 0.35	1102.26	23.00	0.65
E	II	6	-8.06 ± 0.19	1.26 ± 0.43	1.34 ± 0.15	3.57 ± 0.14	15.8 ± 3.64	-3.02 ± 0.32	1088.53	31.84	7.5
F	II	4	-8.03 ± 0.17	1.68 ± 0.38	—	—	16.6 ± 3.4	-3.49 ± 0.34	1106.72	16.51	1.8

Table 2: Best-fit parameters for the model RLFs described in Sec. 5.1. N is the number of free parameters for each model, S is the minimum value of eqn. 10, $\mathrm{Det}(\nabla\nabla S)$ is the determinant of the *Hessian* matrix evaluated at $S = S_{\min}$ and P_{R} is the relative probability of the model calculated according to eqn. 11.

radio spectra of the objects (Sec. 4). We investigated extending our models to include spectral curvature, but concluded that the dataset under study is simply too small to allow the addition of further free parameters to our existing models.

Finally, the reasonably high probability of model F illustrates the effect of the relatively small absolute co-moving volumes observable for the low-redshift counterparts of very rare objects. The co-moving volume available at low-redshift ($z < 1$) is small in comparison to that available in the redshift range $1 < z < 5$ which therefore dominates the total volume available in both cosmologies. For $\beta \sim 1.5$, even with the decrease in the available high-redshift volume caused by the flux-density limit (Fig. 3), we still expect to find a small fraction of the population at low-redshift even if the space density is constant with redshift. We will return to this point in Sec. 8.1 in the context of the results of SH96.

To illustrate the crucial effect of shifting the mean spectral index we re-fitted models C (a cut-off model) and D (a no cut-off model) from Sec. 5.1 assuming a single radio spectral index for the population: we calculated probabilities for $\alpha = 0.0$, the median spectral index of the whole PHJFS sample and the value assumed by SH96, and for $\alpha = 0.2$, the mean α for the most luminous sources In the former case the ratio of probabilities were ~ 50 in favour of a cut-off model, whereas this ratio was ~ 1 when the true mean α was used. This suggests that a parameterisation of the distribution in spectral index is essential to any modelling of the RLF.

To summarise the results of our modelling: the only truly robust feature of the evolutionary behaviour of the most luminous flat-spectrum quasars is a rough constancy in ρ, between $1 \leq z \leq 3.5$. At low-redshift the co-moving volume available is too small in absolute terms to be able to make definitive comments about the space density of rare objects like the most luminous flat-spectrum sources. At higher redshifts, the flux-

density limit eats into the observable volume (Fig. 3) so that again there is insufficient available volume on our light cone to discriminate unequivocally between models with constant ρ and those with arbitrarily sharp high-redshift cut-offs.

6 V/V_{MAX} METHODS

A different method of determining the extent of any evolution in the co-moving space density of radio sources is the $V/V_{\max}$ statistic (Schmidt 1968; Rowan-Robinson, 1968) in which the co-moving volume enclosed by a source is divided by the co-moving volume available to that source given the flux-density limit of the sample and the spectral properties of the source. To dissociate the $V/V_{\max}$ statistic at low-redshift from the high-redshift value we use the banded version of the test (Avni & Bahcall 1980; Avni & Schiller 1983) in which these low- and high-redshift effects are disentangled. If we define V_e as the volume enclosed by a source at the redshift of the source, and V_a as the volume available to this source, given its spectral properties, in a flux-density limited sample then this banded version is given by

$$\left\langle \frac{V_{\mathrm{e}}}{V_{\mathrm{a}}} \right\rangle \rightarrow \left\langle \frac{V_{\mathrm{e}} - V_{\mathrm{o}}}{V_{\mathrm{a}} - V_{\mathrm{o}}} \right\rangle, \tag{12}$$

where $V_\circ$ is the volume enclosed at $z_\circ$.

We find from the banded $V/V_{\max}$ test that between $z \sim 1$ and $z \sim 2$ the points all lie $1 - 2\sigma$ below the value expected for a non-evolving population, dropping to $\approx 2.5\sigma$ below between $2.0 \lesssim z \lesssim 2.4$, before recovering to its previous level up to $z \sim 3.2$. At higher redshifts the lack of sources make it very difficult to accrue any meaningful statistics from this test, particularly as the true error bars are, in the small numbers regime, likely to be larger and less symmetric than those plotted (e.g. Avni & Bahcall 1980).

One likely systematic effect is the curvature of the radio spectra of the radio sources (Savage & Peterson
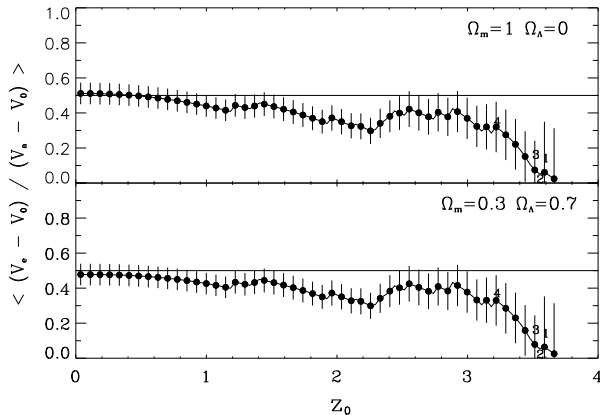
Figure 5: Banded $< V/V_{\mathrm{max}} >$ test for cosmology I (top) and II (bottom) with the effects of spectral curvature explicitly considered. The vertical lines depict $1\sigma = 1/\sqrt{(12N)}$ error bars, where N is the number of sources with redshift $> z_{\circ}$ (see Avni & Bahcall, 1980), and these error bars should be reasonable unless N is small; the redshifts at which $N = 4$, 3, 2 and 1 are marked. The horizontal line at $< (V_{\mathrm{e}} - V_{\mathrm{e}})/(V_{\mathrm{a}} - V_{\circ}) > = 0.5$ corresponds to the mean value for a random distribution of sources throughout the observed co-moving volume.

1983). P85 has mentioned that it is possible to incorporate curvature into a banded V/V_{max} analysis by reducing the available volume to account for a limiting redshift beyond which a source with a given concave spectral shape would be classified as 'steep spectrum' according to a selection criterion based on an observed spectral index. This is clearly a factor deserving consideration, but so too is how, more generally, this curvature will affect the observable volume: the available volume on our light cone will normally be decreased because the observed flux-density of any source with a fixed rest-frame luminosity drops more rapidly with redshift if it has a concave spectrum than if it has a straight spectrum. Our reading of the V/V_{max} analyses of P85 and DP90 papers suggests that these effects have not been fully accounted for, presumably because of the lack of data on curvature in the radio spectra of the sources in the samples under consideration.

Our analysis of the radio spectra of the high-luminosity PHJFS sources (Sec. 4) has allowed us to fully incorporate curvature effects into the banded V/V_{max} test. We did this for each source as follows: we evaluated the 2.7-GHz rest-frame luminosity using the observed flux-density and a polynomial fit to the radio spectrum; we calculate from this two limiting redshifts, one at which a source of the same intrinsic (rest-frame) properties would have a flux-density at the survey limit, and one at which the observed spectrum would become steeper than the survey selection criterion; we then calculate the available volume using the lower of the two different determinations of critical redshift. The results

of this banded V/V_{max} test (with spectral curvature explicitly considered) are plotted in Fig. 5. We find that the systematic shift upwards in V/V_{max} due to curvature effects is extremely small (less than the symbol size in Fig. 5), so P85 and DP90 were justified in neglecting it. There is thus, robust evidence at the $\approx 2\sigma$ level for a significant decline from the banded V/V_{max} test: at $z \sim 2.2$ the statistic is below the critical line at the $\sim 2.5\sigma$ level, although it approaches this line again at $z \sim 3$. The significance of the drop at higher redshifts is still subject to worries over small number statistics.

In summary, there appears to be evidence for a high-redshift decline at the $\sim 2\sigma$ level. This is in quantitative agreement with our likelihood analysis of Sec. 5 where we found a ratio of 10:1 in favour of model E with a cut-off at $z \sim 3.5$, over models without a cut-off: a Gaussian probability distribution falls to $\sim 1/10$ of its peak value roughly 2σ away from the location of the peak. We also find that spectral curvature has a very small but systematic effect on the V/V_{max} statistic which moves it towards the level corresponding to a randomly distributed sample; as we will discuss in Sec. 10.1, this effect may become important when probing out to $z > 5$.

7 CONSTRAINING THE UNCERTAINTIES OF ANY HIGH-REDSHIFT DECLINE

To further quantify the significance of any high-redshift cut-off we have modified the parametric modelling of Sec. 5.1 and used additional variants of the V/V_{max} test used in Sec. 6.

The modified likelihood analysis assumes a very simple high-redshift distribution of the form

$$\rho_z(z) \propto \left(\frac{1+z}{1+z_{\mathrm{peak}}} \right)^{\eta}, \qquad (13)$$

in which we fix the peak redshift $z_{\mathrm{peak}} = 2.5$, and use the fitted values given in Table. 2 for the luminosity function β, the spectral index distribution γ and ϵ. We find the probability distribution function (pdf) for η by integrating over all values of the normalisation parameter $\rho_{\circ}$, i.e.

$$P(\eta \,|\, \mathrm{data}) = \int P(\mathrm{data} \,|\, \log_{10} \rho_{\circ}, \eta) \times$$
$$P(\log_{10} \rho_{\circ}) \, \mathrm{d}(\log_{10} \rho_{\circ}), \qquad (14)$$

where $P(\mathrm{data} \,|\, \log_{10} \rho_{\circ}, \eta)$ is proportional to the likelihood function, $\mathcal{L} \propto \exp^{-S/2}$, and we have assumed a uniform prior for η. S is found by minimising eqn. 10 with a luminosity function ρ of the form,

$$\rho = \rho_{\circ} \times \rho_L(L_{2.7}) \times \rho_{\alpha}(\alpha) \times \left(\frac{1+z}{1+z_{\mathrm{peak}}} \right)^{\eta}. \qquad (15)$$

Note that this is an approximation because we are fixing the majority of the parameters and only integrating over

$\rho_\circ$. However this is reasonable in this case as the fixed parameters will not be as strongly correlated with η as $\rho_\circ$.

Fig. 6 shows the pdf determined for γ from this maximum likelihood method. The area under the curve at $\eta \geq 0$ indicates that there is a detection of a decline above $z \geq 2.5$ with 95% confidence. Thus, although one cannot unequivocally rule out a constant co-moving space density using this method, it is in quantitative agreement with the methods of Sec. 5 and Sec. 6, and highly suggestive of some high-redshift decline. We also estimate the probability of the very abrupt decline ($\eta \approx -6.5$; corresponding to a ~ 1.5 dex decline between $z \sim 2.5$ and $z \sim 5$) preferred by SH98. We find from the area under the curve that this is ruled out with 92% confidence. Thus, although we cannot rule out a decline as abrupt as that envisaged by SH96 and SH98, we find it is disfavoured. The peak of the distribution agrees with a shallow decline reminiscent of the results of DP90. However, the presence of spectral curvature has been neglected by this method which as we now demonstrate systematically shifts the distribution to less negative values of η.
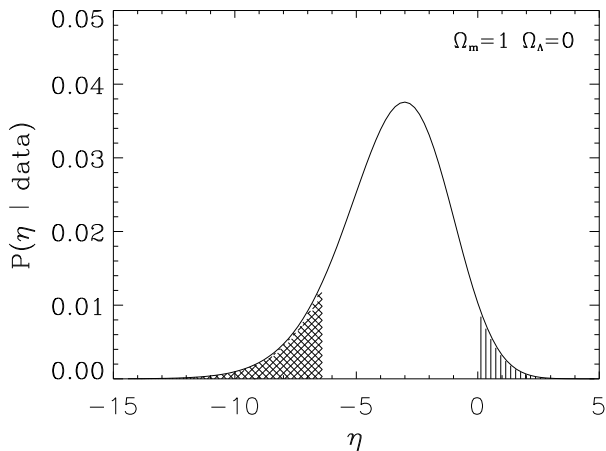

Figure 6: The probability distribution for η from the maximum likelihood method of Sec. 7, adopting cosmology I. The meshed region corresponds to the region where η is steeper than or equal to the abrupt decline preferred by SH96 and SH98; the region shaded with vertical lines corresponds to the values of η where there is either a constant or increasing co-moving space density.

To quantify the effect of spectral curvature we again turn to a variant of the V/V_{max} test discussed by Avni & Bahcall (1980). We use a weighted V/V_{max} statistic, i.e.

$$< A >= \frac{\int_{V_\circ}^{V_e} \rho_z(z) \mathrm{d}V}{\int_{V_\circ}^{V_a} \rho_z(z) \mathrm{d}V}, \qquad (16)$$

where $\rho_z(z)$ is again given by eqn. 13, $V_\circ$ is the volume

η	Weighted V/V_{max}	P_{KS}	Cosmology	Curvature
-6.50	0.64 ± 0.10	0.41	I	No
-3.66	0.50 ± 0.10	0.56	I	No
0.00	0.24 ± 0.10	0.15	I	No
-6.50	0.67 ± 0.10	0.31	I	Yes
-2.77	0.50 ± 0.10	0.57	I	Yes
0.00	0.34 ± 0.10	0.44	I	Yes
-6.50	0.64 ± 0.10	0.41	II	No
-3.64	0.50 ± 0.10	0.56	II	No
0.00	0.25 ± 0.10	0.17	II	No
-6.50	0.66 ± 0.10	0.32	II	Yes
-2.73	0.50 ± 0.10	0.57	II	Yes
0.00	0.35 ± 0.10	0.45	II	Yes

Table 3: Results of the weighted V/V_{max} tests described in Sec. 6.
$\eta_{max} = -3.66^{+1.47}_{-1.83}$ with no curvature for cosmology I.
$\eta_{max} = -2.77^{+1.74}_{-2.04}$ with curvature for cosmology I.
$\eta_{max} = -3.64^{+1.51}_{-1.86}$ with no curvature for cosmology II.
$\eta_{max} = -2.73^{+1.79}_{-2.08}$ with curvature for cosmology II.
The upper and lower limits on η_{max} have been calculated according to the prescription of Avni & Bahcall (1980), in which values of η are evaluated 1σ away from the mean V/V_{max}, again assuming Gaussian errors with a standard deviation $\sigma = (\sqrt{12N})^{-1}$.

enclosed at the peak redshift (again set at $z = 2.5$), V_e and V_a are the volume enclosed by the source and the volume available to the source respectively. Following Avni & Bahcall (1980), we calculate this statistic as a function of η and determine a best-fit value at the point $< A >= 0.5$. The results of this investigation, with and without taking spectral curvature into account, are presented in Table 3.

It is obvious from Table 3 that accounting for spectral curvature changes the best-fit slightly, favouring a more gradual drop in the value of ρ at high redshifts, but does not remove the evidence for a decline. We conclude that a gentle decline in ρ, amounting to a factor ~ 4 from $z \sim 2.5$ to $z \sim 5$, is favoured by the data, with both constant space density models and abrupt cut-off models ruled out at roughly the 2σ level.

8   DISCUSSION

8.1   Understanding the differences between the DP90 and SH96 results

In Fig. 7a we have compared our set of parametric models (Sec. 5) with the results of the free-form analysis of DP90 (for the top decade of their flat-spectrum RLF), and the binned evaluation of SH96. Our models A and E look very like the SH96 points, and our models B and D look very like the DP90 results. Although our
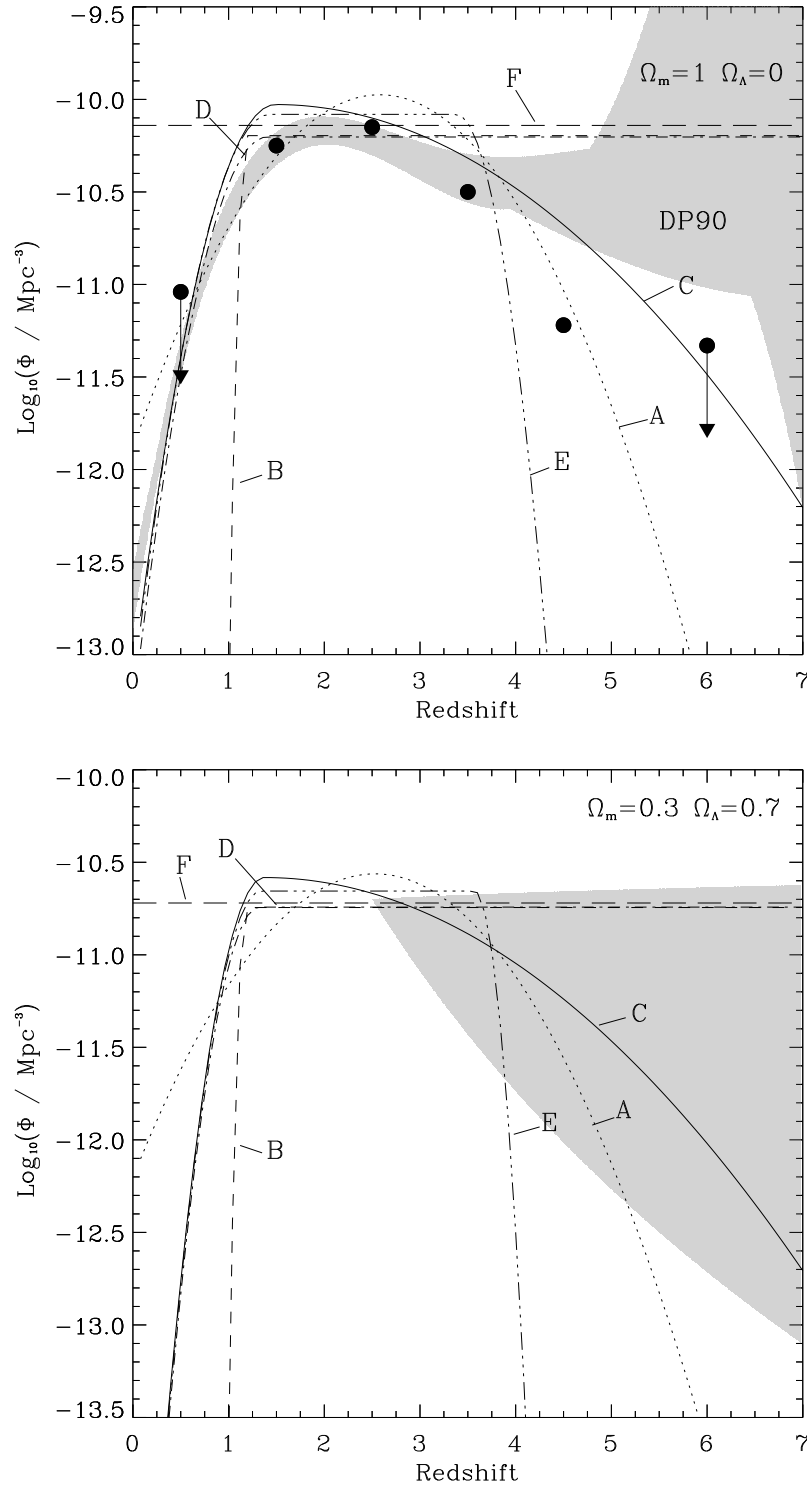
Figure 7: (a) top: The co-moving space density Φ ($\int \int \int \rho \, \mathrm{d}(\log_{10} L_{2.7}) \mathrm{d}z \mathrm{d}\alpha$) for the six model radio luminosity functions described in Sec. 5.1 for cosmology I. The range of free-form RLF models considered by DP90 are also shown by the shaded region for cosmology I. The filled circles show the binned points of SH98 which were calculated assuming $\alpha = 0$ and using a binned method; note the points at $z = 0.5$ and $z = 6.5$ are upper limits which correspond to finding one object at these redshifts. (b) bottom: The co-moving space density for the six model RLFs described in Sec. 5.1 for cosmology II. The shaded region corresponds to the 90 per cent confidence region of the high-redshift space density of quasars using the $V/V_{\max}$ method with curvature included as discussed in Sec. 7.

analysis of Secs. 5, 6 and 7 suggest that it is currently not possible to discriminate unequivocally between these very different high-redshift behaviours, it does lead us to be confident (at the ~ 95 % level) that the DP90 results are the more reliable. The abruptness of the decline suggested by SH96 and SH98 seems likely to be the result of three factors: (i) use of $\alpha = 0$ as a representative spectral index, whereas the most luminous flat-spectrum sources are significantly steeper; (ii) use of a binned method which does not fully account for the steepness of the RLF across the bin which is particularly important at high-redshift where the flux-density limit cuts into the observable volume; and (iii) no corrections for radio spectral curvature. These systematic effects have been discussed in detail in Secs. 3 and 4, and since they all work in the same direction it seems clear that they can combine to produce values of ρ which are systematically biased to low values, possibly by a large factor.

The band of DP90 free-form models diverges rapidly at high-redshifts, but seem at face-value to rule out a very rapid decline (declining by at most a factor ~ 3 between $z = 2.5$ and $z = 5$). Our analysis (Secs. 6 and 7) has attempted to assign probabilities to the strength of this decline which, considering a 90% confidence interval, allow a fairly broad range of declines at high-redshift (see Fig. 7b). Since the direct constraints on the top decade of the RLF are very similar between this work and DP90 (see e.g. Table 1 and Fig. 9 of DP90), this is simply an artifact of differences between our method and the free-form method of DP90.

All likelihood methods applicable to sparsely populated datasets (like those considered here) require some assumption of smoothness, be it a simple functional form (Sec. 5) or a series expansion (DP90). This means that there will be cross-talk between the $\log_{10}(L_{2.7})$-z range of interest and other parts of the $\log_{10}(L_{2.7})$-z plane. The worry is that if, for example, the top decade of the RLF was dominated by a physically-different phenomenon to the rest of the RLF; then cross-talk could introduce abhorrent features into the RLF under investigation. In Secs. 8.2 and 9 we will show that this may be a real concern.

However, cross-talk can be beneficial, as the following discussion illustrates. Consider the low-redshift part of Fig. 7. Both the binned analysis of SH96 and the DP90 modelling suggest very firm evidence for a decline at low-redshifts, whereas the reasonably high relative likelihood of our model F (Sec. 5.2) seems to require no such behaviour. The difference between the SH96 point and our model F can no longer be ascribed to the systematic effects discussed in Secs. 3 and 4 since, as illustrated by Fig. 3, all the most radio-luminous flat-spectrum sources on our light cone are detectable in the area surveyed. The difference is largely due to small number statistics. The ratio of volumes between the SH96 redshift bins centred at 0.5 and 1.5 is about 1/3

(cosmology II) [§], so from Table 2 and the assumption of a fairly constant ρ, ~ 2 sources would be predicted in the low-redshift bin whereas zero are seen. This has a Poisson probability ($\sim e^{-2} = 0.13$), and its true significance must also allow for Poisson noise in the upper redshift bin (which accounts for the drop in the normalisation of model F with respect to the other models), so that as a detection of a 'low-redshift' cut-off it is not particularly significant. However, the tight constraints on the DP90 models give firm evidence for a significant low-redshift decline, and although this is an artifact of cross-talk, it is almost certainly true. The reason for this is as follows: if we were to gradually lower the critical luminosity (arbitrarily) defining our 'most radio luminous' sub-set, then the number of such sources at low-redshift would increase rapidly by virtue of the steep radio luminosity function; in a repeated binned analysis, the effects of Poisson noise could be marginalised, illustrating a beneficial effect of the cross-talk inherent in the DP90 method.

The crucial point is that similar arguments – namely solving the problem of small number statistics by extending the study to include lower luminosity objects – are not applicable in anything like the same straightforward manner to any high-redshift cut-off. The situation is greatly complicated by the truncations enforced on the observable volume by the existence of flux-density selection limits (see Secs. 3 and 4, particularly Fig. 3). Because of these truncations, the search for low luminosity objects at high-redshifts requires the use of fainter samples. The work of DP90 utilised $L_{2.7} - z$ data from a fainter sample (see Table 1) which did allow some sensitivity to less radio luminous objects at high-redshift, but because of the small sky area of this sample, the total number of $z > 2$ flat-spectrum sources in their study is similar to that in the PHJFS sub-set studied here. Given this fact, and given that a significant fraction of sources are common to both studies (Sec. 2) it is no surprise that, for example, their $V/V_{\max}$ analysis yields strikingly similar results (compare Fig. 5 with Fig. 12 of DP90). We note also the worrying incompleteness of the faintest DP90 sample near the flux-density limit (DP90 Appendix A): this is a particular problem for interpreting low values of $V/V_{\max}$ as evidence for a high-redshift cut-off, since objects with high values of $V/V_{\max}$ will always lie near the flux-density limit of a survey, and if these sources are in the top-decade of the RLF they must be at high-redshift.

[§] This is the one calculation in this paper where the difference between cosmologies I and II has an important effect, so we prefer the one currently favoured by observations (e.g. Perlmutter et al. 1999). The *relative* co-moving volumes between two redshift bins are relatively large if the bins are at low- and high-redshift, but small if both bins are at high-redshift (which is always the case for the most luminous PHJFS sources considered in this paper).

To conclude this section we contend that the evidence against models with constant space density at high-redshift, or indeed a cut-off as abrupt as that envisaged by SH96 and SH98, is not yet compelling. The evidence for any cut-off at high-redshift for flat-spectrum sources is at present significant only at the $\sim 2\sigma$ level, and therefore in our view still tentative. However, the best bet, as quantified in Fig. 7b and Table 3 and as previously suggested by P85 and DP90, is that such a cut-off does exist, and amounts to a gradual decline in ρ by a factor ~ 4 between redshifts $z \sim 2.5$ and $z \sim 5$.

8.2 Linking the most luminous flat-spectrum quasars with the steep-spectrum population

The most common physical cause of a flat radio spectrum at $\sim 1\,$GHz frequencies is synchrotron self-absorption implying that the emission comes from compact regions. This means that there are at least two distinct ways in which the steep- and the flat-spectrum populations could be linked. The first way concerns the early phases of radio source evolution in which the emission comes from regions so compact that a Giga-Hertz Peaked radio Spectrum (GPS) inevitably results. Current theories (see review by O'Dea 1998) suggest that all FRII (Fanaroff-Riley class II; Fanaroff & Riley 1973) radio sources (before developing their large-scale steep-spectrum lobes) pass through a GPS phase, and move through a Compact Symmetric Object (CSO) phase as the source further expands and its turnover frequency drops. The second way concerns sources favourably oriented such that the emission from the base of one of their jets is beamed along the line-of-sight, producing Doppler-Boosted (DB), or 'core-dominated', sources (e.g. Blandford & Rees 1978). We will consider these two possibilities in turn.

To what part of the steep-spectrum population would GPS sources with $\log_{10}(L_{2.7}) > 27$ correspond? There are two strong lines of argument that for a given source $L_{2.7}$ must decline steadily with time. First assuming that the environmental density declines with radius, any reasonable model for source expansion (e.g. Begelman 1996; Kaiser & Alexander 1997; Blundell, Rawlings & Willott 1999; Blundell & Rawlings 1999) predicts this must be the case. Secondly, if the luminosity was constant or increased with time then the known GPS sources would dramatically over-produce FRIIs. A synthesis of these ideas (O'Dea & Baum 1997) suggests that $L_{2.7} \propto D^{-0.5}$, so that in growing out of the GPS phase (at a size ~ 0.3 kpc) into a FRII (of size ~ 300 kpc), $L_{2.7}$ declines by a factor $\sim 10^{1.5}$, and since the source will now be optically thin at much lower frequencies we can extrapolate this value (using $\alpha = 0.8$) to obtain $L_{151} = 26.5$. This is well above the FRI/FRII break, so the most-luminous GPS sources seem certain to become FRIIs, and they lie at or just above the L_{151}

boundary at which the quasar fraction of FRIIs drops precipitously (e.g. Willott et al. 2000a). Measurements of the RLF suggest that sources of this L_{151} have a space density $\log_{10} \rho \sim -6.5$ at $z \sim 2.5$ (Willott et al. 2000b; DP90), roughly 3 dex higher than the value of ρ inferred for the $\log_{10}(L_{2.7}) > 27$ flat-spectrum population. We therefore have no difficulty linking this population with the $\log_{10}(L_{151}) \lesssim 26.5$ FRIIs providing the GPS phase persists for a time which is $\sim 10^3$-times shorter than the FRII phase. This seems plausible since estimates of the kinematical ages of FRII radio sources, based on lobe asymmetries and light travel-time effects, gives a value $\sim 10^{7.5}$ yr for a 500-kpc FRII (e.g. Scheuer 1995), whereas a direct measurement of the expansion rate of a GPS source by Owsianik & Conway (1998) suggests a kinematical age in the range 10^{3-4} yr.

To what part of the steep-spectrum population would DB sources with $\log_{10}(L_{2.7}) > 27$ correspond? An attempt to unify the flat- and steep-populations via Doppler boosting has recently been made by Jackson & Wall (1999). They find that to produce flat-spectrum sources from a parent FRII requires that the jets have a bulk Lorentz factor $\gamma \approx 8.5$, and requires that the jets are aligned within a critical angle $\theta_{\rm crit} \approx 7°$ of the line-of-sight. These values set a characteristic Doppler factor[¶] $\Gamma \sim 10$ for the luminous flat-spectrum sources, and hence predict a boosting of the core flux by a factor $\Gamma^2|_{\theta=\theta_{\rm crit}}/\Gamma^2|_{\theta=\theta_{\rm trans}} \sim 10^3$ in a comparison between flat spectrum objects and their counterparts aligned at the transition angle $\theta_{\rm trans}$ where, according to unified schemes, the quasar nucleus just becomes optically visible (we take $\theta_{\rm trans} \approx 53°$ from Willott et al. 2000a). Measured core-to-lobe ratios R at high radio frequencies are $\sim 10^{-1.5}$ for objects marking the division between quasars and radio galaxies, i.e. those aligned at $\theta \approx \theta_{\rm trans}$ (see Fig. 8 of Jackson & Wall 1999). For DB sources the core is likely to be boosted to a flux-density much ($\sim 10^{1.5}$) higher than the (presumably roughly isotropic) high-frequency flux-density of the lobe. This means that a $\log_{10}(L_{2.7}) > 27$ source will have a lobe with $\log_{10}(L_{2.7}) \gtrsim 25.5$, or (taking $\alpha = 0.8$) $\log_{10}(L_{151}) \gtrsim 26.5$. In other words, we expect both the GPS and DB populations to be drawn from similar parts of the RLF of the FRII population, one dex above the FRI/FRII divide, and about at the point where the observed quasar fraction switches from ≈ 0.1 to ≈ 0.4 (Willott et al. 2000a). As for the GPS objects, the DB objects will be drawn from a population with a space density $\log_{10} \rho \sim -6.5$ at $z \sim 2.5$ (Willott et al. 2000, DP90), but this time it is a small beaming angle, rather than a small source age which lies behind the lower derived ρ for the flat-spectrum popu-

---

[¶] Doppler factor $\Gamma = \gamma^{-1}(1 - \beta\cos\theta)^{-1}$, where β is the speed (in units of c) of the bulk motion and θ is the angle of the motion with respect to the line-of-sight.

lation. Taking $\theta = 7°$ means that only ~ 1 in ~ 200 sources is expected to be favourably oriented, but this still slightly over-produces the observed flat-spectrum population at $\log_{10}(L_{2.7}) > 27$. There are enough uncertainties in this argument that this is not a serious problem: for example, adopting a slightly lower characteristic Doppler factor would allow us to associate the DB objects with slightly more radio luminous FRII parents, say $\log_{10}(L_{151}) \gtrsim 27$, and thus resolve the problem. An important corollary of these ideas will be discussed in Sec. 10.2.

With the possibility of a mixed GPS and DB population in mind, the obvious next step was to turn our attention to the radio properties of the $\log_{10}(L_{2.7}) > 27$ PHJFS sample. In Fig. 4 we have shown radio spectra of each object, together with rough spectral classifications. Simple inspection shows that in several cases where the data are adequate, the spectra are characteristic of GPS or CSS sources (four of these objects are in the O'Dea review on GPS sources and 2 others are present in the GPS sample of de Vries, Barthel & O'Dea 1997). Few of the spectra bear much resemblance to the compilation of DB objects of Gear et al.(1994) which typically peak around 10 GHz and decline at higher frequencies. The nature of the minority of objects with straight or concave spectra is unclear, although they are reminiscent of the Core-Jet Sources (CJS) mentioned by Willott et al. (1998), the archetype being 3C286, which, having jet structures on *both* sides of the nucleus, are believed to be dominated by a component which lacks strong Doppler boosting.
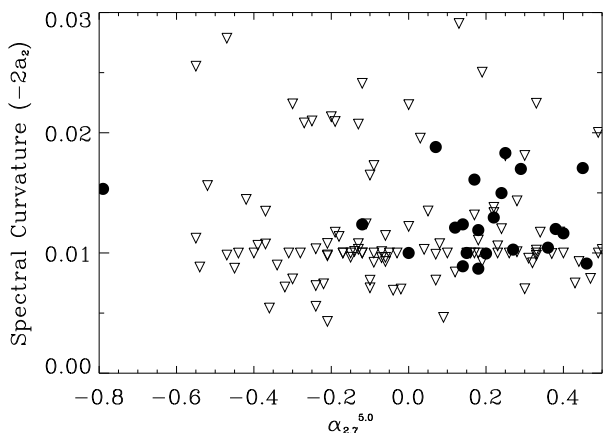

Figure 8: The distribution in the curvature $(-2a_2)$ of radio spectra as a function of $\alpha_{2.7}^{5.0}$ for the most luminous PHJFS sources (filled circles) and sources from the next lower decade in radio (2.7 GHz) luminosity (triangles).

To pursue this qualitative result, we plot in Fig. 8 the curvature $(-2a_2$, where a_2 is defined in Sec. 4) of the radio spectrum against observed radio spectral index for the most luminous PHJFS sub-set, and the PHJFS sources from the next lower dex in radio lu-

minosity. The shift in observed spectral index for the most radio-luminous sources (Sec. 3) is clearly shown in this plot, but we also see hints that the spectral curvatures are significantly different for the most luminous subset (naive application of the 1-D KS test yields $P_{KS} = 0.02$ for the distributions in spectral curvature of the two samples, with median curvature $-2a_2 = +0.34$ in the top decade and $-2a_2 = -0.14$ in the next lower decade). It is not possible to make more definitive statements from this plot because the radio data used to construct the radio spectra are rather inhomogeneous (we have compiled them using data from the Nasa Extragalactic Database), particularly in terms of their frequency coverage: some of the objects may be characterised as having straight spectra $(-2a_2 \sim 0)$, or highly curved spectra, merely because of the lack of many frequency points in their radio spectra and/or time variability. However, it does seems clear that there are a significant number of GPS sources in the top decade of the flat-spectrum RLF, and more arguably they seem to form a lower fraction of the population at lower radio luminosities. Accepting these arguments allows us to tie up two loose ends. First, the shift towards steeper radio spectra in this decade (Fig. 2) can now be understood as the emergence of a population of GPS source with turnover frequencies in the rest-frame GHz range, and hence characteristically steeper spectra at an observed frequency of 2.7 GHz. Second, the worries concerning cross-talk between lower parts of the RLF, and its top decade (Sec. 10.1) inherent in any analysis assuming a smooth continuous RLF appear to be worthy of further investigation. As we will show in Sec. 10.2 a significant ratio of GPS-like sources to DB sources is likely to be restricted to a fairly narrow range of 2.7 GHz luminosity so extrapolations of any properties, including space density, must be pursued with extreme care in the overlap region between the two physically distinct populations.

9   FLAT-SPECTRUM QUASAR EVOLUTION IN A COSMOLOGICAL CONTEXT

In Sec. 7 we discussed that the evidence of any decline in the ρ of flat-spectrum quasars at high-redshifts is rather gentle compared to the evolutions preferred by the analyses of SH96 and SH98. This is entirely consistent with constraints on the high-redshift evolution in ρ for the steep-spectrum population to which, as argued in Sec. 8.2, this flat-spectrum population is ultimately linked. Willott et al. (1998) have determined that quasars with $\log_{10}(L_{151}) \gtrsim 27$ rise in space density by ~ 2 dex between $z \sim 0$ and $z \sim 2$, but then stay at roughly constant ρ out to $z \sim 3$, beyond this redshift the evolution in ρ remains poorly constrained. This mirrors the behaviour of the entire FRII population at these luminosities (DP90, Willott et al. 2000b) which

is unsurprising given that the quasar fraction shows no dependence on radio luminosity at $\log_{10}(L_{151}) > 26.5$ (Willott et al. 2000a). Efforts targeted at mapping the high-redshift cut-off of the steep-spectrum population have yet to find any evidence of a high-redshift decline in the ρ of the steep-spectrum FRII population (Rawlings et al. 1998; Jarvis et al 1999; Willott et al. 2000b; Jarvis et al. 2000), but are consistent with a gentle decline in ρ (as favoured for the flat-spectrum population in this paper and in DP90).

How does this situation compare to the cosmic evolution of optically-selected quasars? It has now been established that the optical luminosity function (OLF) is steep ($\beta \sim 1.5$) with an increase in ρ by ≈ 2 dex out to $z \sim 2.2$ (e.g. Goldshmidt & Miller 1998). At higher redshifts, despite their different selection techniques, several surveys have now yielded fairly consistent results favouring a significant decline at high redshift: Warren, Hewett & Osmer (1994) from a multicolour survey, Schmidt, Schneider & Gunn (1995) using quasars discovered by their Lyα emission, Hawkins & Veron (1996) using a variability technique, and Kennefick, Djorgovski & de Carvalho (1995) using a multicolour technique have all argued for an abrupt decline in ρ between $z \sim 2.5$ and $z \sim 4$. As shown on Fig. 2 of SH96, these results are all consistent with a decline in ρ by a factor ~ 10 between $z \sim 2.5$ and $z \sim 5$. $^\parallel$ Comparing the redshift cut-off of optically-selected quasars with the cut-off for flat-spectrum radio quasars, as put forward here and in DP90, suggests that the drop in ρ is more abrupt for the optically-selected population than for the radio-selected population, whereas SH96 and SH98 argued that the declines are similar. One obvious way in which ρ might drop more rapidly for optically-selected quasars than for radio-selected quasars would be if there is an increasing chance of dust obscuration at high-redshift, either dust in intervening systems (e.g. Fall & Pei 1989), or dust associated with their young host galaxies.

X-ray surveys of quasars provide another probe of evolutions in ρ. Both Boyle et al. (1994) and Page et al. (1996) successfully fitted a pure luminosity evolution (PLE) model to the X-ray luminosity function (XLF)

$^\parallel$ A contrary view has been put forward by Irwin, McMahon & Hazard (1991) who discussed evidence that ρ for the optically brightest quasars is roughly constant between $z \sim 2$ and $z \sim 4.5$. The optical and UV spectra of quasars are far more complex than the relatively simple radio spectra studied in this paper, and uncertainty in K-corrections could lead to complications in determining the absolute magnitude of sources needed to correctly place quasars at various redshifts from various samples onto the steep OLF. So, just as $K-$corrections were vital in understanding the discrepancies between previous determinations of the flat-spectrum RLF (Sec. 7), this may also prove to be the case for optically-selected quasars. As emphasised recently by Wolf et al. (1999), different optical selection techniques for quasars may also need to be explored.

with the evolution slowing down, but not necessarily reversing above a redshift $z \sim 1.7$. The most recent results by Miyaji et al. (2000), using just *ROSAT* observations to avoid cross-calibration problems, found similar behaviour, and no evidence for any high-redshift cut-off. Our results of Sec. 7 show that any discrepancy between the high-redshift evolution of X-ray selected quasars and flat-spectrum radio quasars which were highlighted by Miyaji et al. (2000) are resolvable within the uncertainties of both samples.

In a still wider cosmological context, the redshift cut-off of active galaxies has been linked to the cosmic evolution in the global star-formation rate (e.g. SH98). The most recent studies of the global high-redshift star-formation rate based on (dust corrected) optical data (Steidel et al. 1999) and on sub-mm data (e.g. Blain et al. 1999, Eales et al. 1999, Hughes et al. 1998) are now in reasonable accord: the Steidel et al. study finds no significant change in the luminosity function of Lyman-break galaxies between redshifts $z \approx 3$ to $z \approx 4$, and thus no evidence yet for a high-redshift decline in global star formation. Our results of Sec. 7 remove any significant difference between global star formation and the evolution of flat-spectrum radio sources, as the form of the high-redshift evolution in both cases is consistent within the uncertainties. Differences inferred from comparing the Steidel et al. work and optically-selected quasars are probably robust (see e.g. Cen 2000) but arguably now should be discussed in the context of possible dust obscuration of the optically-selected quasar population at high redshift.

10 CAN THE REDSHIFT CUT-OFF FOR FLAT-SPECTRUM QUASARS EVER BE FIRMLY ESTABLISHED?

10.1 The top decade of the flat-spectrum RLF

We first assess the chances of establishing beyond doubt a redshift cut-off using just the most luminous flat-spectrum quasars. The SH96 approach to this problem was to search for $z > 5$ quasars in their faintest 2.7-GHz radio survey which has a flux-density limit of $S_{2.7} > 0.25 \, \mathrm{Jy}$ (see Table 1). They found no $z > 5$ quasars, and in SH98 say that if there was no fall-off in the space density of quasars at high-redshift, they would have expected to find 15 quasars at $5 < z < 7$.

We will compare the predictions of models C and D from Sec. 5, the former having a fairly gradual decline at high-redshift, and the latter having a co-moving space density which remains constant above a peak $z^{\star\star}$. The

---

** The results of this section do not depend critically on the assumed cosmological model for the reasons discussed in Sec. 8.1; we use Cosmology I

high-redshift behaviour of these models roughly correspond to the ~ 90 per cent confidence interval derived in Sec. 7 and plotted on Fig. 7b.

We have made Monte Carlo simulations of a survey similar to the Parkes-based work of SH96 and SH98, i.e. a 2.7-GHz flux-density limit of 0.25 Jy over a sky area of 3.8 sr with a spectral index selection criterion $\alpha_{2.7}^{5.0} \le 0.4$. These simulations show that we would expect on average to find 0.3 objects with $\log_{10}(L_{2.7}) \ge 27$ in the redshift range $5 \le z \le 7$ for model C and 4 objects for model D. The corresponding numbers of quasars predicted in the $4 \le z \le 5$ range are 1.5 (model C) and 4 (model D). If we now account for the mean spectral curvature of the sources, as described in Sec. 4, and re-run the simulations we predict 0.1 quasars with $5 \le z \le 7$ (and 0.5 with $4 \le z \le 5$) for model C, and now only 1 with $5 \le z \le 7$ (and 1.6 with $4 \le z \le 5$) for model D.[††] Such numbers represent a tiny fraction of the ~ 1000 flat-spectrum sources in the survey, but are consistent with a previous estimate (Dunlop et al. 1986) that ~ 0.5 per cent of the Parkes flat-spectrum sources lie at $z > 4$ (this estimate was based on a gradual redshift cut-off very similar to the one preferred by the analysis of Sec. 7, but did not account for spectral curvature). For a no cut-off model our predicted numbers of high-redshift quasars are an order-of-magnitude lower than the SH98 estimate of 15 quasars at $z > 5$; we believe this to be a good illustration of the significance of the biases discussed at length in Secs. 3 and 4.

These simulations show that even restricting our attention to two specific models, small number statistics preclude any definitive statement on the cut-off since the probability of detecting zero $z > 5$ objects in the no cut-off case is given by the Poisson probability $\sim e^{-1} \approx 0.35$. Therefore, even if the SH96 survey was extended to the whole sky, and it was certain that it included no $z > 5$ quasars, then one could only rule out model D at roughly the 95 per cent level by using the most luminous sources.

We conclude that the observable volume in the high-redshift Universe is simply too small to delineate the redshift cut-off using objects as rare as the flat-spectrum quasars *in the top decade of the RLF*.

10.2   Less luminous flat-spectrum sources

We next assess the chances of delineating the cut-off by analysing redshift surveys at fainter flux-density limits. We consider first the GPS sources, which we argued in Sec. 8.2 are an important population within the top decade of the flat-spectrum RLF. GPS sources in this

luminosity regime should be the progenitors of FRII radio sources with 151 MHz luminosities $\log_{10}(L_{151}) \sim 26.5$, so to estimate the number of GPS sources in fainter samples we need to consider how the steep-spectrum RLF behaves at lower values of L_{151}. At $z \sim 2$ the steep-spectrum RLF is constrained by the radio source counts to flatten considerably below $\log_{10}(L_{151}) \sim 27$ (Willott et al. 1998; Willott et al. 2000b), so that lowering the flux-density limit by say a factor of ten, would increase the number of high-redshift GPS quasars in a given sky area by a factor of a few rather than by orders-of-magnitude. Direct evidence in favour of this argument comes from the GPS survey at faint (~ 0.05 Jy) flux-density by Snellen et al. (1998,1999) which has found 13 GPS quasars with a similar redshift distribution to those found in Table 1, representing a surface density ~ 20 sr^{-1}, i.e. a factor ~ 4 higher than the surface density of the most luminous sources in the PHJFS sample. Therefore, although the huge effort of surveying the whole sky for GPS sources could increase the number of objects in the high-redshift Universe considerably, and thus improve constraints on the cut-off, the gains would be small enough that small number statistics would remain a crucial limitation.

There is also an argument that the importance of GPS sources within the $\log_{10}(L_{2.7}) > 27$ population might swiftly reverse to complete dominance by the DB population over the next lowest decade. It would be pure fluke if the FRII counterparts of the DB and GPS populations had precisely the same characteristic value of $\log_{10}(L_{151})$ for a given value of $\log_{10}(L_{2.7})$. If, as seems likely (Sec. 8.2) the DB objects are on average drawn from higher up the FRII RLF, then the number of these will increase more rapidly with decreasing $L_{2.7}$ than would be the case for GPS sources. We have presented tentative evidence that this is actually the case in Sec. 8.2. This means that studies of the cut-off with samples dominated by DB objects, and with much less severe problems due to small number statistics, may be plausible at lower flux-density levels.

Of course DP90 have made the first stab at just such an experiment, but we have argued in Sec. 10.1 that among other problems the sky area of their faintest sample was insufficient to add much to constraints available from the bright sample data (P85; this paper). The DP90 analysis also does not account for the change over from a mixed population of GPS and DB sources in the top decade, to mainly DB sources in the next lower decade. A new analysis that separates these distinct populations and that takes careful account of $K-$corrections is probably warranted, and in the longer term, a large increase in survey area is highly desirable. The higher values of ρ for the $\log_{10}(L_{2.7}) \sim 26 - 27$ DB population means that the volume on our light cone in the high-redshift Universe is sufficient to eliminate the problem of small number statistics given a suffi-

---

[††] It is worth noting that, although the effects of spectral curvature on the derived evolution in co-moving space densities were shown to be systematic but small in Sec. 6, they become increasingly important as the properties of the population are extrapolated to larger redshifts.

ciently wide-area redshift survey. Selection of samples of flat-spectrum sources should probably incorporate low-frequency survey data to avoid missing objects with spectra which are intrinsically flat at ∼GHz frequencies, but which appear steep because their spectra are highly redshifted.

11 ACKNOWLEDGEMENTS

REFERENCES

Antonucci R.R.J., 1993, ARAA, 31, 473
Avni Y. & Bahcall J.N., 1980, ApJ, 235, 694
Avni Y. & Schiller N., 1983, ApJ, 267, 1
Begelman M.C., 1996, Cygnus A - study of a radio galaxy, Proc. of the Greenbank Workshop, eds. Carilli C.L.; Harris D.E., 209, CUP
Blain A.W., Smail I., Ivison R.J., Kneib J-P., 1999, MNRAS, 302, 632
Blandford R. & Rees M.J., 1978, in Wolfe A.M., ed., Pittsburgh Conference on BL Lac Objects, Univ. Pittsburgh, p.328
Blundell K.M. & Rawlings S.R., 1999, Nature, 399, 330
Blundell K.M., Rawlings S., Willott C.J., 1999, AJ, 117, 677
Boyle B.J., Shanks T., Georgantopoulos I., Stewart G.C. & Griffiths R.E., 1994, MNRAS, 271, 639
Boyle B.J. & Terlevich R.J., 1998, MNRAS, 293, 49
Cen R., 2000, ApJL, in press, astro-ph/0002425
de Vries W.H., Barthel P.D., O'Dea C.P., 1997, A&A, 321, 105
Drinkwater M.J., Webster R.L., Francis P.J., Condon J.J., Ellison S.L., Jauncey D.L., Lovell J., Peterson B.A., Savage A., 1997, MNRAS, 284, 85
Dunlop J.S., 1998, in Observational Cosmology with the New Radio Surveys, eds. M.N. Bremer et al., 157, Kluwer
Dunlop J.S., Downes A.J.B., Peacock J.A., Savage A., Lilly S.J., Watson F.G. & Longair M.S., 1986, Nature, 319, 564
Dunlop J.S.& Peacock J.A., 1990, MNRAS, 247, 19
Eales S. et al., 1999, ApJ, 515, 518
Efstathiou G. & Rees M.J., 1988, MNRAS, 230, 5
Ellingson E., Green R.F., Yee H.K.C., 1991, ApJ, 378, 476
Fall S. & Pei Y.C., 1989, ApJ, 337, 7
Fanaroff B.L., & Riley J.M., 1974, MNRAS, 167, 31
Gear W.K. et al., 1994, MNRAS, 267, 167
Goldschmidt P. & Miller L., 1998, MNRAS, 293, 107
Haiman Z. & Loeb A., ApJ, 1997, 483, 21
Hawkins M.R.S., Veron P., 1996, MNRAS, 281, 348
Hughes D.H., et al., 1998, Nature, 394, 241
Irwin M., McMahon R. & Hazard, C., 1991, in The Space Distribution of Quasars, ed. Crampton, ASPCS21, 117
Jackson C.A. & Wall J.V., 1999, MNRAS, 304, 160

Jarvis M.J., Rawlings S., Willott C.J., Blundell K.M., Eales S.A., Lacy M., 1999, in The Hy-redshift universe: Galaxy formation and evolution at high redshift' eds. A.J. Bunker and W.J.M. van Breugel
Jarvis M.J., Rawlings S., Willott C.J., Blundell K.M., Eales S.A., Lacy M., 2000, MNRAS, submitted
Kaiser C.R. & Alexander P., 1997, MNRAS, 286, 215
Kennefick J.D., Djorgovski S.G. & de Carvalho, R.R., 1995, AJ, 110, 2553
Madau P., Ferguson H.C., Dickinson M.E., Giavalisco M., Steidel C.C. & Fruchter A., 1996, MNRAS, 283, 1388
Marshall H.L., Avni Y., Tanenbaum H., Zamorani G., 1983, ApJ, 269, 35
Miyaji T., Hasinger G., Schmidt M., 2000, A&A, 353, 25
O'Dea C.P., 1998, PASP, 110, 493
O'Dea C.P. & Baum S.A., 1997, AJ, 113, 148
Owsianik I., Conway J.E., 1998, A&A, 337, 69
Page M.J., Carrera F.J., Hasinger G., Mason K.O., McMahon R.G., Mittaz J.P.D., Barcons X., Carballo R., Gonzalez-Serrano I., Perez-Fournon I., 1996, MNRAS, 281, 579
Peacock J.A., 1983, MNRAS, 202, 615
Peacock J.A., 1985, MNRAS, 217, 601
Peacock J.A. & Gull S.F., 1981, MNRAS, 196, 611
Peacock J.A. & Wall J.V., 1981, MNRAS, 194, 331
Percival W.J., & Miller L., 1999, MNRAS, 309, 823
Perlmutter S. et al., 1999, ApJ, 517, 565
Press W.H., Teukolsky S.A., Vetterling W.T., Flannery B.P., 1992, Numerical Recipes: The Art of Scietific Computing. CUP, Cambridge
Rawlings S., Blundell K.M., Lacy M., Willott C.J., Eales S.A., 1998, in Observational Cosmology with the New Radio Surveys, eds. M.N. Bremer et al., 171, Kluwer
Rees M.J., 1995, Perspectives in Astrophysical Cosmology, CUP
Rowan-Robinson M.M., 1968, MNRAS, 138, 445
Sandage A., 1972, ApJ, 178, 25
Savage A., Peterson B.A., 1983, IAUS, 104, 57
Scheuer P.A.G., 1995, MNRAS, 277, 331
Schmidt M., 1968, ApJ, 151, 393
Schmidt M., Schneider D.P. & Gunn J.E., 1995, AJ, 110, 68
Shaver P., Hook I.M., Jackson C.A., Wall J.V., Kellermann K.I., 1998, in Highly Redshifted Radio Lines, eds. C.Carilli, S.Radford, K.Menten & G.Langston
Shaver P.A., Wall J.V., Kellermann K.I., Jackson C.A., Hawkins M.R.S., 1996, Nature, 384, 439
Sivia D.S., 1996, Data Analysis: A Bayesian Tutorial, OUP
Snellen I.A.G., Schilizzi R.T., Bremer M.N., Miley G.K., de Bruyn A.G., Röttgering H.J., 1999, MNRAS, 307, 149
Snellen I.A.G., Schilizzi R.T., de Bruyn A.G., Miley G.K., Rengelink R.B., Röttgering H.J., Bremer M.N., 1998, A&AS, 131, 435
Steidel C.C., Adelberger K.L., Giavalisco M., Dickinson M., Pettini M., 1999, ApJ, 519, 1
Valageas P. & Silk J., 1999, A&A, 347, 1
Wall J.V., 1998, in Observational Cosmology with the New Radio Surveys, eds. M.N. Bremer et al., 129, Kluwer
Wall J.V. & Jackson C.A., 1997, MNRAS, 290, L17
Wall J.V. & Peacock J.A., 1985, MNRAS, 216, 173
Warren S.J., Hewett P.C. & Osmer P.S., 1994, ApJ, 421, 412
Willott C.J., Rawlings S., Blundell K.M., Lacy M., 1998, MNRAS, 300, 625
Willott C.J., Rawlings S., Blundell K.M., Lacy M., 2000a, MNRAS, in press (astro-ph/0003461)
Willott C.J., Rawlings S., Blundell K.M., Lacy M., Eales S.A., 2000b, MNRAS, submitted
Wolf C., Meisenheimer K., Roser H.-J., Beckwith S.V.W., Fockenbrock R., Hippelein H., von Kuhlmann B., Phleps S., Thommes E., 1999, A&A, 343, 399